Journal of Power Sources 196 (2011) 8789–8801

Contents lists available at ScienceDirect

Journal of Power Sources

journal homepage: www.elsevier.com/locate/jpowsour

# Influences of temperature, $H_2SO_4$ concentration and Sn content on corrosion behaviors of PbSn alloy in sulfuric acid solution

D.G. Li*, D.R. Chen, J.D. Wang, H.S. Chen

*State Key Laboratory of Tribology, Tsinghua University, Beijing, 100084, China*

ARTICLE INFO

*Article history:*
Received 10 May 2011
Received in revised form 8 June 2011
Accepted 23 June 2011
Available online 29 June 2011

*Keywords:*
PbSn alloy
Cyclic voltammetry (CV)
A.c. voltammetry (ACV)
Mott–Schottky analysis
Electrochemical impedance spectra

ABSTRACT

The influences of temperature, $H_2SO_4$ concentration and Sn content on corrosion behaviors of PbSn alloys in sulfuric acid solution were investigated by potentiodynamic curve, cyclic voltammetry (CV), linear sweeping voltage (LSV), electrochemical impedance spectra (EIS), a.c. voltammetry (ACV) and Mott–Schottky analysis. The microstructure of the corrosion layer on PbSn alloy was analyzed by scanning electron microscopy (SEM). The results showed that the corrosion resistance of PbSn alloy increased with ascending Sn content and $H_2SO_4$ concentration, the increment of temperature can decrease the corrosion resistance of PbSn alloy in $H_2SO_4$ solution. The conductivity of the anodic film on PbSn alloy was enhanced with increasing temperature, ascending Sn content and descending $H_2SO_4$ concentration. SEM result revealed that the corrosion film after cyclic voltammetry was consisted of tetragonal crystal, the porosity enlarged with decreasing temperature, Sn content and $H_2SO_4$ concentration.



## 1. Introduction

Generally, lead and lead alloy were widely used as the grid material of the lead acid battery due to their good anti-corrosion performance in sulfuric acid solution [1–10]. The good anti-corrosion behaviors of lead or lead alloy were attributed to the passive film on the substrate, the passive film can act as the ions barrier between the aggressive electrolyte and the substrate, and therefore slow down the corrosion rate obviously. Different to passive films on other alloys, passive films formed on lead or lead alloy in sulfuric acid solution have three characteristics: firstly, the passive film should have good protection on the substrate considering the operation environment of the grid in lead acid battery; secondly, the passive film should also have good electronic conductive property, as the passive film exists between the active material and substrate, better electronic conductivity of the passive film better charging–discharging performance of lead acid battery is; thirdly, when lead or lead alloy is polarized at positive potential, a semi-permeable film $PbSO_4$ is firstly formed, which only permits $H^+$, $OH^-$ and $H_2O$ diffusion but not $Pb^{2+}$ and $SO_4^{2-}$, the lead oxides are formed under the semi-permeable film, especially for PbO film, which has quite high resistivity (about $10^{11}\ \Omega\,cm^2$) [1], hence to impede the electronic conduction through the grid/active material interface and lead to the premature capacity loss of the lead acid battery [11–15]. In order to alleviate the premature capacity loss, Sn was added into the grid alloy, it is reported that Sn can significantly improve the film conduction by the formation the $PbO_{1+x}$ ($0 < x < 1$) [16,17], but some researchers found that the addition of Sn can accelerate the self-discharge and grid corrosion [18,19]. In the factual environment, lead acid battery may be suffering the temperature change, the electrolyte concentration in lead acid battery may be varied with increasing the operation time. While fewer papers focused on the influences of $H_2SO_4$ concentration and temperature on the corrosion behaviors of lead alloys in sulfuric acid solution.

This paper aimed to investigate the influences of temperature, $H_2SO_4$ concentration and Sn content on corrosion behaviors of PbSn alloy in sulfuric acid by potentiodynamic curve, linear sweeping voltage (LSV), cyclic voltammetry (CV), electrochemical impedance spectra (EIS) and Mott–Schottky plot, the microstructure of the corrosion film after CV was observed by scanning electron microscopy (SEM).

## 2. Experimental

PbSn alloys were prepared by melting weight mixtures of pure lead (99.99 wt.%) and pure tin (99.99 wt.%) in a vaccum furnace. The Sn contents of PbSn alloys were 0.8, 1.78 and 2.1 wt.%, respectively. PbSn alloys were embedded in two-component epoxy resin and mounted in a PCV holder, the exposed face of the electrode

* Corresponding author. Tel.: +86 10 6279 5148; fax: +86 10 6278 1379.
*E-mail address:* dgli@mail.tsinghua.edu.cn (D.G. Li).

0378-7753/$ – see front matter 
doi:10.1016/j.jpowsour.2011.06.082

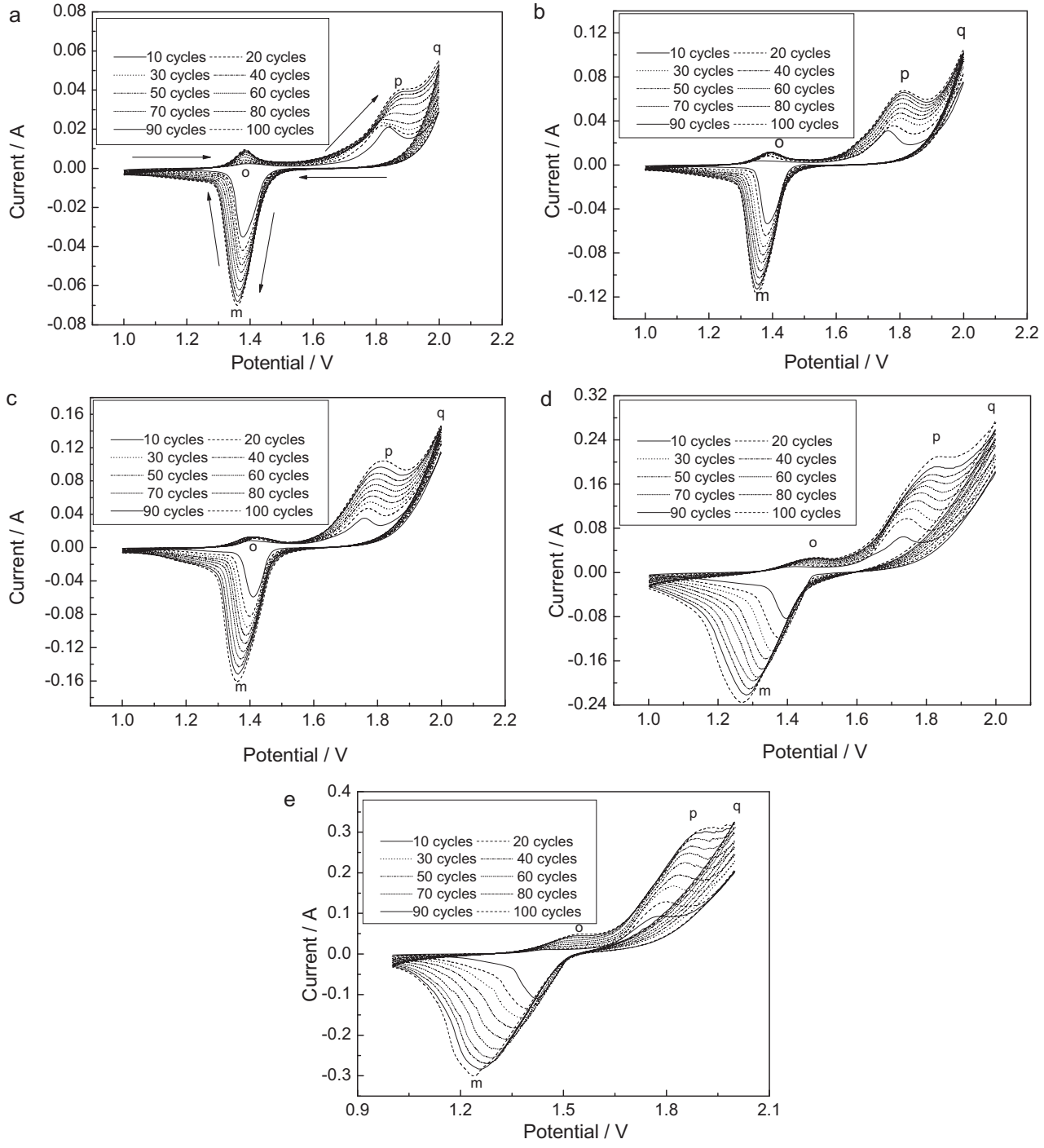


**Fig. 1.** Cyclic voltammetry of Pb0.8Sn alloy in 4.5 M $H_2SO_4$ solution at different temperatures (a) 25 °C, (b) 40 °C, (c) 55 °C, (d) 70 °C and (e) 85 °C.

with a geometric area of 0.7856 $cm^2$, was abraded with 2000 grit SiC paper, polished with 0.5 μm $Al_2O_3$ powder, and cleaned using double-distilled water. After being washed and dried, the electrode was submitted to a cathodic treatment at $-1.2V_{ocp}$ for 20 min to reduce previous films formed in the air on the surface of the working electrode.

A conventional three-electrode system was used, the counter electrode was a Pt wire with an area of 2 cm × 2 cm, and all potentials were measured against a saturated calomel electrode (SCE). Cyclic voltammetry (CV), linear sweep voltammetry (LSV), a.c. voltammetry (ACV) experiments were performed using CH Instrument Model 750 electrochemical working station, EIS and Mott–Schottky analysis were carried out at EG and G Model M273A electrochemical working station. The electrolyte solutions used in this work were prepared from double distilled water and analytical grade reagents as follows: 0.5 mol $L^{-1}$ $H_2SO_4$, 1.5 mol $L^{-1}$ $H_2SO_4$, 2.5 mol $L^{-1}$ $H_2SO_4$, 3.5 mol $L^{-1}$ $H_2SO_4$ and 4.5 mol $L^{-1}$ $H_2SO_4$.

For cyclic voltammetry, the sweeping voltage was from 1 V to 2 V with a scanning rate of 10 mV $S^{-1}$, and the cyclic number was 100.

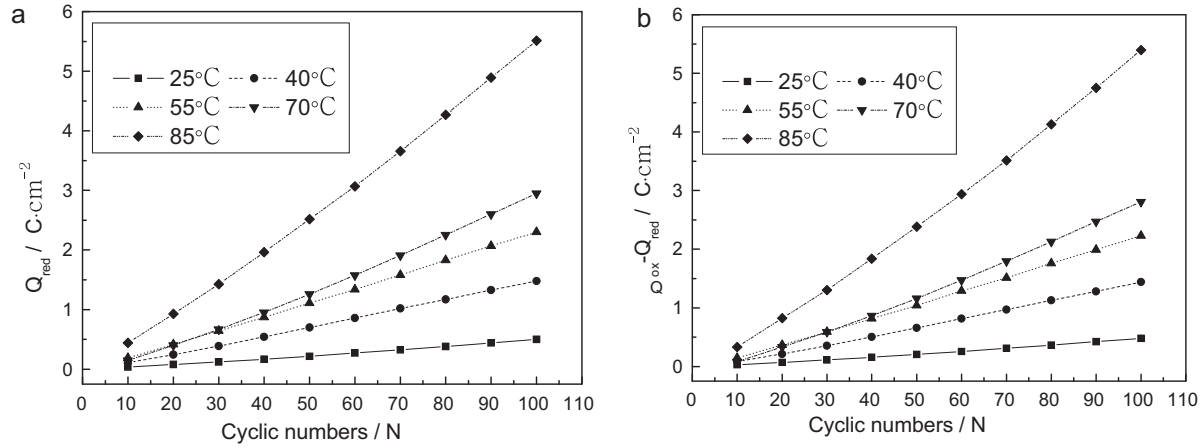


**Fig. 2.** $Q_{red}$ and $Q_{ox} - Q_{red}$ verse cyclic numbers for corrosion films formed on Pb0.8Sn alloy in 4.5 M $H_2SO_4$ solution at different temperatures, (a) $Q_{red}$ verse cyclic number plot and (b) $Q_{ox} - Q_{red}$ verse cyclic number plot.

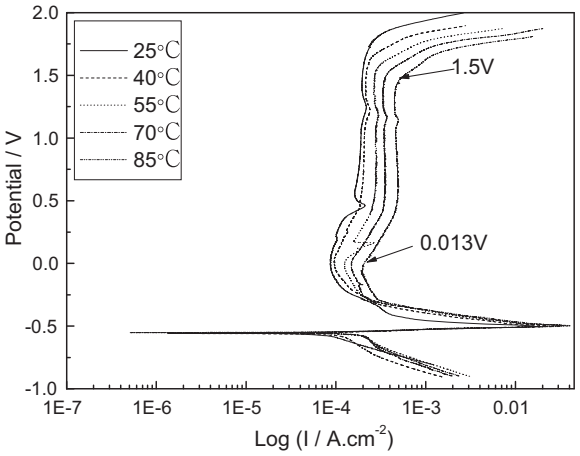


**Fig. 3.** The potentiodynamic curves of Pb0.8Sn in 4.5 M $H_2SO_4$ solution at different temperatures.

For linear sweep voltammetry (LSV), the anodic film was firstly formed at 1.28 V for 2 h in 4.5 mol $L^{-1}$ $H_2SO_4$ solution, then the working electrode was immediately scanned from 1.28 V to −1.0 V with a rate of 2 mV $S^{-1}$.

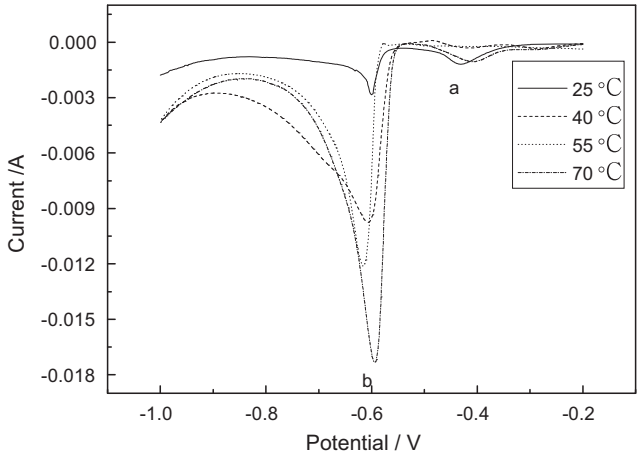


**Fig. 4.** The linear sweeping voltammetries of anodic films on Pb0.8Sn electrode at different temperatures.

For a.c. voltammetry, the anodic film was firstly formed at 1.28 V for 2 h in 4.5 mol $L^{-1}$ $H_2SO_4$ solution, then the frequency of 1000 Hz was used to record the change of the real part of the impedance ($Z'$) for the anodic film with the voltage.

For EIS experiment, the sweeping frequency was from 100 kHz to 10 mHz with an increased potential of 10 mV, the measured potential was 0 V (verse open circuit potential), and the impedance spectra was fitted by Zsimpwin software.

Mott–Schottky plot was performed within the potential region of −0.5 V to 1.5 V with a 5 mV $s^{-1}$ scanning rate, and the measured frequency was 1 kHz.

The temperature effect on the potential was corrected using the following formula [20]:

$$E_t = E_{25}^{\Phi} + 0.871(t - 25) \quad (1)$$

where $t$ was the celsius degree.

## 3. Results and discussions

### 3.1. Temperature effect on corrosion behaviors of Pb in sulfuric acid solution

#### 3.1.1. Cyclic voltammetry (CV)

Fig. 1 shows the cyclic voltammetries of Pb0.8Sn electrode for 100 cycles performed between 1 V and 2 V with a sweep rate of 10 mV $S^{-1}$ in 4.5 mol $L^{-1}$ $H_2SO_4$ solution at different temperatures.

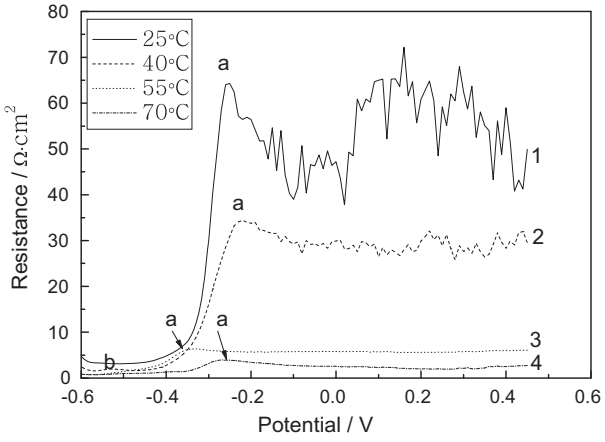


**Fig. 5.** The a.c. voltammetries of the anodic films on Pb0.8Sn alloy at 1.28 V for 2 h in 4.5 M $H_2SO_4$ solution at different temperatures.

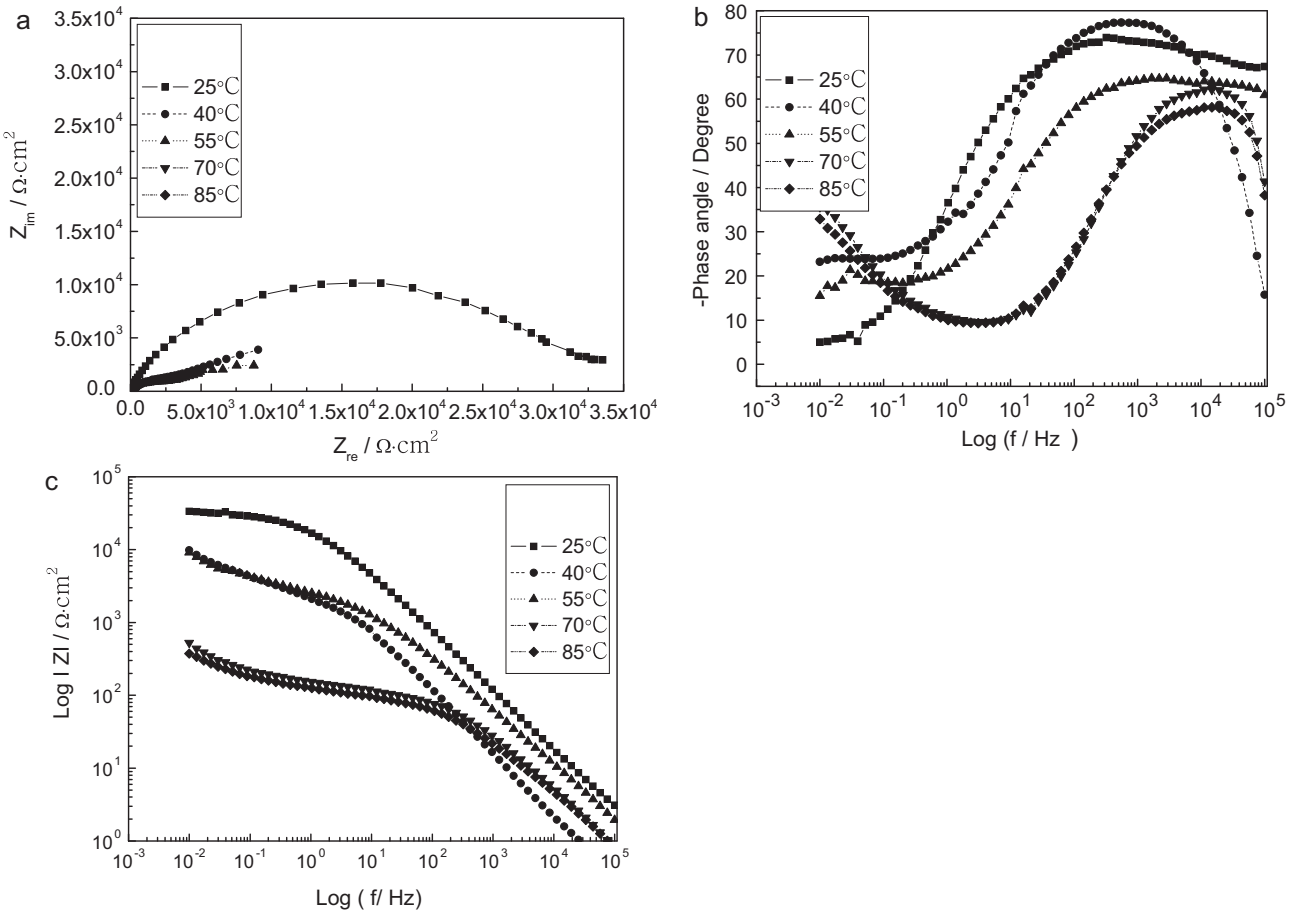


**Fig. 6.** The impedance spectra of the anodic films formed on Pb0.8Sn alloy at 1.28 V for 2 h in 4.5 M $H_2SO_4$ solution at different temperatures, (a) Nyquist plot; (b) corresponding Bode phase angle and Bode impedance magnitude (c) plots.

It can be seen that the cyclic voltammetries displayed similar features, i.e., in the positive scanning process, three peaks donated as o, p and q can be observed, beginning at about 1.38 V, 1.84 V, and 2.0 V, respectively. Furthermore, a large cathodic peak m was formed at about 1.36 V. In which peak o was associated with the oxidation of the inner PbO, $PbSO_4$ and matrix lead into α-$PbO_2$, peak p was related to the formation of β-$PbO_2$ from $PbSO_4$, and peak q corresponded to the oxygen evolution. In the cathodic scanning, peak m represented the reduction of α-$PbO_2$ into $PbSO_4$ [21]. Additionally, the peak currents increased with the increment of the cycles, the reason can be related to the increased corrosion of the electrode and the increasing specific surface area of the corrosion film with cycle.

Owing to peaks o and p corresponding to the oxidation of Pb(II) to Pb(IV), peak m was related to the reduction of Pb (IV) to Pb(II), we can assume the difference between $Q_{ox}$ and $Q_{red}$ may be due to the anodic evolution of oxygen. Fig. 2 gives the variations of $Q_{red}$ and $Q_{ox} - Q_{red}$ with the cyclic number, it can be observed that there were good linear relationships between $Q_{red}/Q_{ox} - Q_{red}$ and the cyclic numbers ($N$), the slopes increased with the increment of temperature, indicating the improved corrosion behavior and increased oxygen evolution for Pb0.8Sn alloy in 4.5 M $H_2SO_4$ solution.

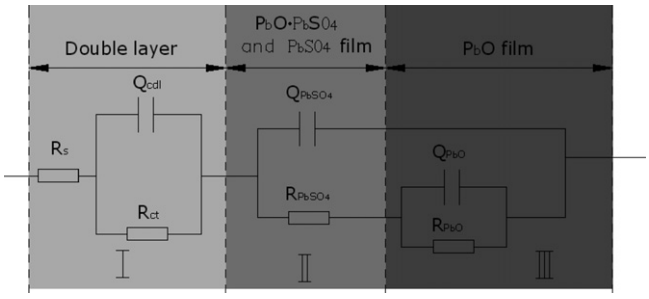


**Fig. 7.** The corresponding equivalent circuits used for fitting the impedance data.

### 3.1.2. Potentiodynamic curve

The potentiodynamic curves of Pb0.8Sn electrode in 4.5 M $H_2SO_4$ solution at different temperatures are shown in Fig. 3, it can be seen that Pb0.8Sn alloy was in the passive state from about 0.013 V to 1.5 V, the passive state was related to the formation of the protective passive film on PbSn alloy, the passive potential regions significantly decreased with increasing temperature, the steady passive currents at 25 °C, 40 °C, 55 °C, 70 °C and 85 °C were 1.77E−4 A $cm^{-2}$, 2.017E−4 A $cm^{-2}$, 2.796E−4 A $cm^{-2}$, 3.4E−4 A $cm^{-2}$ and 4.711E−4 A $cm^{-2}$, respectively. Obviously, they increased with increasing temperature, it indicated that the protective effect of the anodic film on Pb0.8Sn alloy decreased with temperature.

### 3.1.3. Linear sweeping voltammetry (LSV)

The linear sweeping voltammetries of anodic films formed on Pb0.8Sn electrode at 1.28 V for 2 h in 4.5 M $H_2SO_4$ solution at different temperatures are shown in Fig. 4, it was clear that two reduction peaks can be observed in LSV, in which peak a represented the reduction of Pb(II) (like PbO, PbO·$PbSO_4$, 3PbO·$PbSO_4$, etc.) to Pb and peak b was caused by the reduction of $PbSO_4$ to Pb [22]. The corresponding current of peak b sharply descended, while

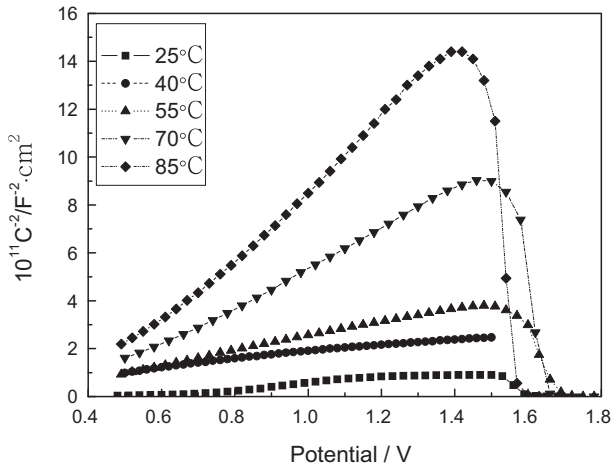


**Fig. 8.** Mott–Schottky plots of anodic films formed on Pb0.8Sn alloy at 1.28 V for 2 h in 4.5 M $H_2SO_4$ solution at different temperatures.

the current of peak a slightly decreased with ascending temperature, therefore, it can be demonstrated that the growth of $PbSO_4$ was enhanced with ascending temperature, the thickness of Pb(II) film (like PbO, PbO·$PbSO_4$, 3PbO·$PbSO_4$, etc.) slightly decreased, the inhibitive growth of PbO indicating a better conductivity of the anodic film with temperature.

### 3.1.4. A.C. voltammetry (ACV)

For grid material, the most important requirement was the good conductivity of the anodic film on its surface, the corrosion film existing between the active material and the grid in lead acid battery played a role of collecting and distributing the currents, therefore, the charge–discharge performance of the battery was determined by the conductivity of the corrosion film. The operation of the lead acid battery may suffer different temperatures in practice, the temperature change may affect the conductivity of the corrosion film on grid surface, and hence to influence the charge–discharge performance of lead acid battery.

Fig. 5 shows the variations of $Z'$ (real part of the impedance spectra of the anodic film) with $E$ for the anodic films on Pb0.8Sn alloy at 1.28 V for 2 h in 4.5 M $H_2SO_4$ solution at different temperatures, it can been obviously seen that the value of $Z'$ decreased from peak a to peak b (1.23 Ω $cm^2$) in curves 1, 2, 3 and 4, respectively. In which, peak a was related to the reduction of the high impedance Pb(II) film to Pb, the values of peak a in curves 1, 2, 3 and 4 were 64.16 Ω $cm^2$, 34.71 Ω $cm^2$, 6.06 Ω $cm^2$ and 3.97 Ω $cm^2$, significantly, it sharply decreased with increasing temperature, implying the better conductivity of the anodic film at 1.28 V at higher temperature, the result was consistent with LSV.

### 3.1.5. Electrochemical impedance spectroscopy (EIS)

The impedance spectra of anodic films on Pb0.8Sn electrode at 1.28 V for 2 h in 4.5 M $H_2SO_4$ solution at different temperatures are depicted in Fig. 6, it was clear from Fig. 6a that the semicircle decreased with the increment of temperature, the Bode plot (Fig. 6b) shows that a shoulder appeared at low frequencies (lower than 1 Hz), which 'splits' the curves into two different frequency regions, clearly pointed to the response of at least two different frequency-dependent processes with corresponding time constants, one constant time which appeared in the frequency region lower than 1 Hz originated from the space charge in the film/metal interface and the other appearing in the frequency region higher than 1 Hz may originated from the film/solution interface. According to Pavlov et al. [16], the anodic film on lead electrode at 1.28 V appeared the structure of Pb/PbO/$PbSO_4$/electrolyte, then,

**Table 1**
The fitted results of the impedance spectra.

| Elements | 25 °C | 40 °C | 55 °C | 70 °C | 85 °C |
|---|---|---|---|---|---|
| $R_s$ (Ω $cm^2$) | 0.4256 | 0.4035 | 0.4911 | 0.5622 | 0.535 |
| $Y_{cdl}$ ($\Omega^{-1}$ $S^n$) | 1.958E−5 | 3.47E−5 | 4.193E−5 | 1.099E−4 | 1.334E−3 |
| $n_{cdl}$ | 1 | 0.7956 | 0.768 | 0.6514 | 0.7427 |
| $R_{ct}$ (Ω $cm^2$) | 1627.2 | 673 | 190.9 | 49.14 | 38.27 |
| $Y_{PbSO_4}$ ($\Omega^{-1}$ $S^n$) | 8.476E−5 | 1.662E−4 | 2.048E−4 | 2.5E−4 | 2.786E−4 |
| $n_{PbSO_4}$ | 0.7986 | 0.7762 | 0.6214 | 1 | 1 |
| $R_{PbSO_4}$ (Ω $cm^2$) | 2.548E4 | 1311 | 440.8 | 100.1 | 40.45 |
| $Y_{PbO}$ ($\Omega^{-1}$ $S^n$) | 1.411E−4 | 1.165E−4 | 1.726E−4 | 1.806E−4 | 1.905E−4 |
| $n_{PbO}$ | 0.938 | 0.7045 | 0.6148 | 0.5681 | 0.5984 |
| $R_{PbO}$ (Ω $cm^2$) | 2.064E4 | 6670 | 195.8 | 121.2 | 95.59 |

the equivalent electron circuit shown in Fig. 7 was provided to fit the EIS spectra, the equivalent electron circuit comprised the constant phase element (CPE) and resistance $R$, in which $R_S$ was the solution resistance, $Q_{cdl}$ was the capacitance of the double layer, $R_{ct}$ was the transfer resistance, $Q_{PbSO_4}$ and $R_{PbSO_4}$ were the capacitance and resistance of the $PbSO_4$ film, $Q_{PbO}$ and $R_{PbO}$ were the capacitance and resistance of the PbO film, respectively. A constant phase element (CPE) was used, the impedance and admittance of CPE can be obtained with the following relationship [23,24].

$$Z_{CPE} = [Y_0(jw)^n]^{-1} \quad (2)$$

$$Y_{CPE} = Y_0(j\omega)^n \quad (3)$$

where $j$ was the imaginary number, $w$ was the frequency of alternative current, exponent $n$ was defined as the CPE power, which was adjusted between 0 and 1. For $n = 1$, the CPE described an ideal capacitor with $Y_0$ equal to the capacitance $C$, for $n = 0$, the CPE was an ideal resistor. When $n = 0.5$, the CPE represented a Warburg impedance with diffusion character, while $0.5 < n < 1$, CPE was the combination of properties related to both the surface and the electroactive species, and exponent $n$ was the slope of the impedance-frequency Bode plot [25]. CPE had the properties of a capacitance when $0.5 < n < 1$, the CPE described a frequency dispersion of time constants due to local inhomogeneous, porosity and roughness of the electrode surface.

The fitted results of the impedance spectra are listed in Table 1, it can be noticed that the resistances of $PbSO_4$ film, PbO film and the transfer resistance decreased, the capacitances of double layer, $PbSO_4$ film and PbO film increased with the increment of temperature, the increment of capacitance and decrement of resistance indicating a rough and inhomogeneous character of the anodic film, it may be concluded that the increased micro-channel within $PbSO_4$ and PbO film with increasing temperature, the ions easily passed through the anodic film, then the conductivity of the anodic film enhanced.

### 3.1.6. Mott–Schottky plot

The Mott–Schottky plot was often used to investigate the electronic properties of passive film on metals by measuring the electrode capacitance as a function of the potential ($E$). The Mott–Schottky plot expressed the relationship of space charge capacitance $C_{sc}$, of a n-type semiconductor and the film-formation potential $E$ as following [26,27]:

$$C^{-2} = C_{sc}^{-2} = \frac{2}{\varepsilon\varepsilon_0 e N_D}\left(E - E_{FB} - \frac{KT}{e}\right) \quad (4)$$

where $\varepsilon$ was the dielectric constant of the passive film, $\varepsilon_0$ was the vacuum permittivity ($8.854 \times 10^{-14}$ F $cm^{-1}$), $e$ was the electron charge, $N_D$ was the donor density. $E_{FB}$ was the flat-band potential, $K$ was the Boltzmann constant, $T$ was the absolute temperature. $KT/e$ can be negligible as it was only about 25 mV at room temperature, $N_D$ can be estimated from the slope of linear fitted M–S plots, while $E_{FB}$ came from the extrapolation for $C_{sc}^{-2} = 0$.

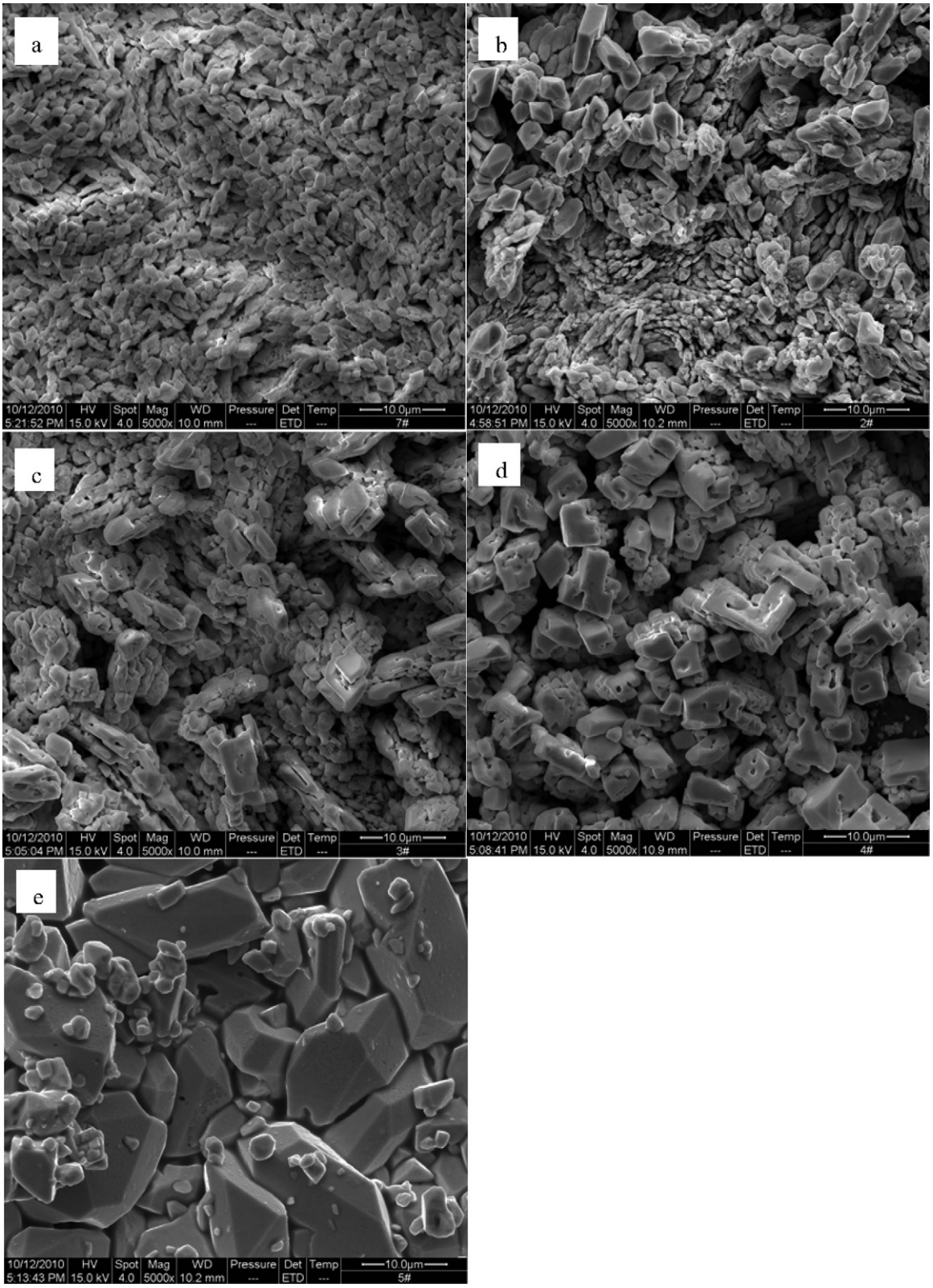


**Fig. 9.** Micro-structure of corrosion films on Pb0.8Sn alloy after CV for 100 cycles in 4.5 M $H_2SO_4$ solution at different temperatures, (a) 25 °C; (b) 40 °C; (c) 55 °C; (d) 70 °C; (e) 85 °C.

The Mott–Schottky plots of anodic films on Pb0.8Sn alloy in 4.5 M $H_2SO_4$ solution at 1.28 V for 2 h is shown in Fig. 8. It can be seen that the slopes of M–S plots exhibited positive, indicating the n-type semi-conductive character. As mentioned above, the major components of the anodic film formed on lead alloy at 1.28 V in sulfuric acid solution was Pb(II) (PbO and $PbSO_4$), PbO was an oxide conductor with interstitial oxygen ($PbO_{1+x}$) based on the crystallography of PbO, therefore, it had p-type semiconductive character. However, the positive slopes of M–S plots meaning the n-type semiconductive performance of the anodic film, herewith, there existing

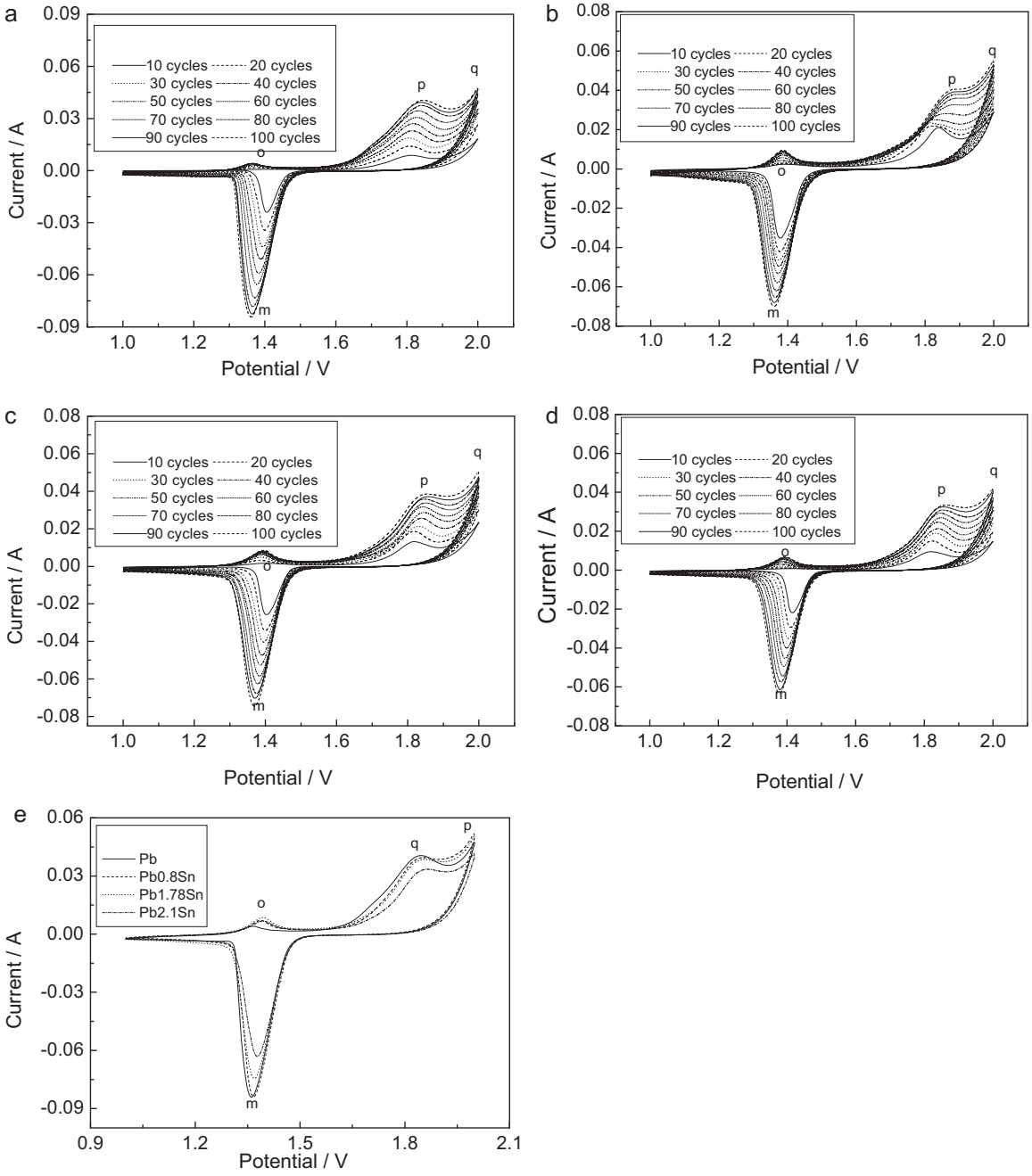


**Fig. 10.** Cyclic voltammetry of PbSn alloy in 4.5 M $H_2SO_4$ solution (a) Pb, (b) Pb0.8Sn, (c) Pb1.78Sn, (d) Pb2.1Sn, (e) cyclic voltammetries of four electrodes after 100th cycle.

the oxides with n-type semi-conductive within the anodic film, comparing with the results of ACV and EIS, the anodic film may be composed of a mixture of PbO and $PbO_2$ ($PbO_{1+x}$) ($PbO_2$ had n-type semiconductive character), which can explain the n-type semiconductive behavior of the anodic film on Pb0.8Sn alloy, this result was also in accordance with Bojinov [28].

### 3.1.7. Microstructures of corrosion films after CV

The micro-structure of corrosion films on Pb0.8Sn alloy after CV for 100 cycles in 4.5 M $H_2SO_4$ solution at different temperatures are displayed in Fig. 9, it can be noticed that the corrosion films appeared tetragonal structure, the size of the crystal significantly increased with increasing temperature, and the porosity of the corrosion film increased, then the ions can easily penetrate the corrosion film, the conductivity and the corrosion of the electrolyte may be enhanced, this was in agreement with the electrochemical experiments.

## 3.2. Influence of Sn content on corrosion behaviors of PbSn alloy in sulfuric acid solution

### 3.2.1. Cyclic voltammetry (CV)

The Sn effect on the cyclic voltammetry of PbSn alloy in 4.5 M $H_2SO_4$ solution is shown in Fig. 10, the cyclic voltammetries of four electrodes displayed similar feature, three peaks donated as o, p and q appeared at about 1.38 V, 1.84 V, and 2.0 V in the positive scanning process and a large cathodic peak m was observed at about 1.36 V, respectively. Analogously, peak o was associated with the oxidation of the inner PbO, $PbSO_4$ and matrix lead into $\alpha$-$PbO_2$, peak p was related to the formation of $\beta$-$PbO_2$ from $PbSO_4$, and

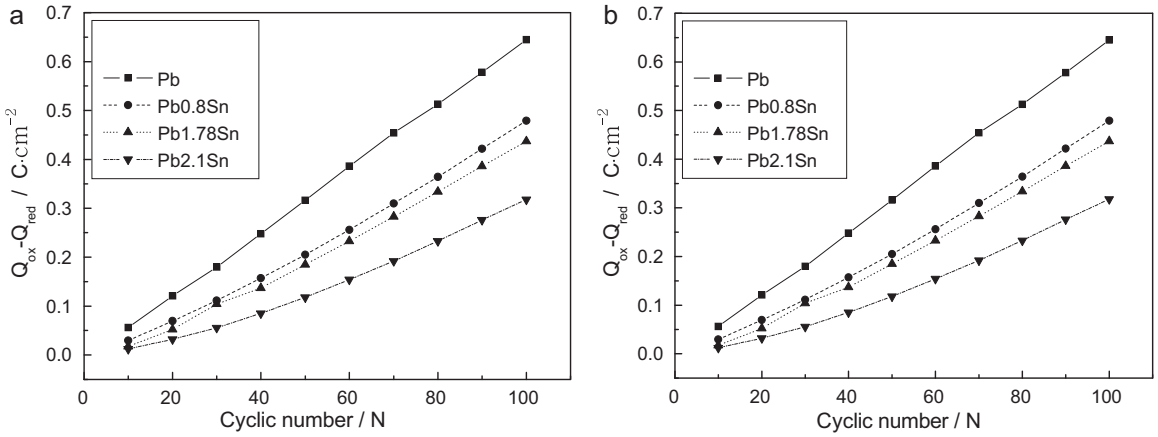


**Fig. 11.** $Q_{red}$ and $Q_{ox} - Q_{red}$ verse cyclic numbers for corrosion films formed on PbSn alloys in 4.5 M $H_2SO_4$ solution, (a) $Q_{red}$ verse cyclic number plot, (b) $Q_{ox} - Q_{red}$ verse cyclic number plot.

peak q corresponded to the oxygen evolution, peak m represented the reduction of α-$PbO_2$ into $PbSO_4$. Fig. 10e shows that three peaks (o, p and m) currents increased with the increment of the cycles, implying the increased corrosion with cycle.

Similarly, Fig. 11 are the variations of $Q_{red}$ and $Q_{ox} - Q_{red}$ with cyclic number, evidently, a good linear relationship between $Q_{red}$ or $Q_{ox} - Q_{red}$ and cyclic number can be observed, the slopes decreased with the increment of Sn content, it revealed that the corrosion and the oxygen evolution of PbSn alloy were inhibited by increasing Sn content.

### 3.2.2. Potentiodynamic curve

The influence of Sn content on potentiodynamic curves of PbSn alloys in 4.5 M $H_2SO_4$ solution is shown in Fig. 12, it manifested that Pb, Pb0.8Sn, Pb1.78Sn and Pb2.1Sn electrodes were in the passive state from about 0.094 V to 1.711 V in 4.5 M $H_2SO_4$ solution, the passive potential regions were almost constant, the steady passive currents for Pb, Pb0.8Sn, Pb1.78Sn and Pb2.1Sn electrodes were 2.265E−4 A $cm^{-2}$, 1.77E−4 A $cm^{-2}$, 1.672E−4 A $cm^{-2}$ and 1.303E−4 A $cm^{-2}$, respectively. Evidently, the steady passive current declined with increasing Sn content, it indicated that the increment of Sn content in the substrate can enhance the film protection.

### 3.2.3. Linear sweeping voltammetry (LSV)

Fig. 13 shows the linear sweeping voltammetries of anodic films on Pb, Pb0.8Sn, Pb1.78Sn and Pb2.1Sn alloys at 1.28 V for 2 h in 4.5 M $H_2SO_4$ solution, similarly, two reduction peaks a and b appeared in LSV, it clearly showed that the corresponding currents of peaks a and b decreased with increasing Sn content. As peaks a and b were corresponding to the reduction of Pb(II) (like PbO, PbO·$PbSO_4$, 3PbO·$PbSO_4$, etc.) and $PbSO_4$ to Pb, respectively, the decrement of peak current demonstrated that growth of Pb(II) in the corrosion film was inhibited by adding Sn, the inhibitive growth of Pb(II) implied the increased conductivity of the anodic film on PbSn alloy with increasing Sn content.

### 3.2.4. A.C. voltage (ACV)

Fig. 14 shows the a.c. voltammetries of anodic films on four electrodes at 1.28 V for 2 h, it evidently revealed that the value of $Z'$ (real part of the impedance spectra of the anodic film) decreased from peak a to peak b (1.23 Ω $cm^2$) in curves 1, 2, 3 and 4, respectively. As illustrated above, peak a was related to the reduction of the high impedance Pb(II) film to Pb, the values of peak a in curves 1, 2, 3 and 4 were 86.07 Ω $cm^2$, 64.16 Ω $cm^2$, 13.26 Ω $cm^2$ and 11.18 Ω $cm^2$, respectively. Significantly, it sharply decreased with increasing Sn content, implying the better conductivity of the anodic film at 1.28 V by increasing Sn content, the reason may be attributed to Sn increased the oxidation process of PbO to $PbO_n$ ($1 < n < 2$) and prevented the formation of tet-PbO [5,29].

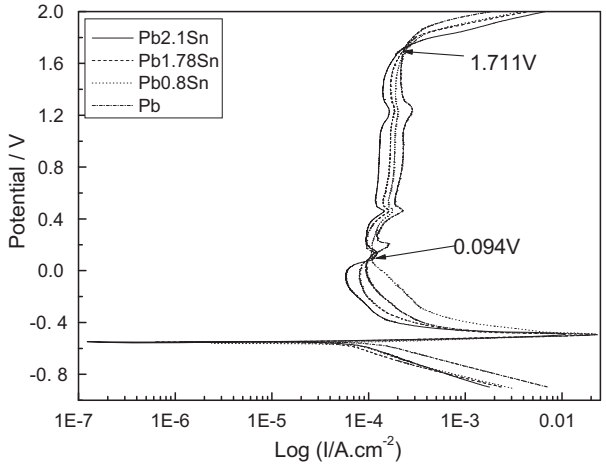


**Fig. 12.** The potentiodynamic curves of Pb, Pb0.8Sn, Pb1.78Sn and Pb2.1Sn electrodes in 4.5 M $H_2SO_4$ solution.

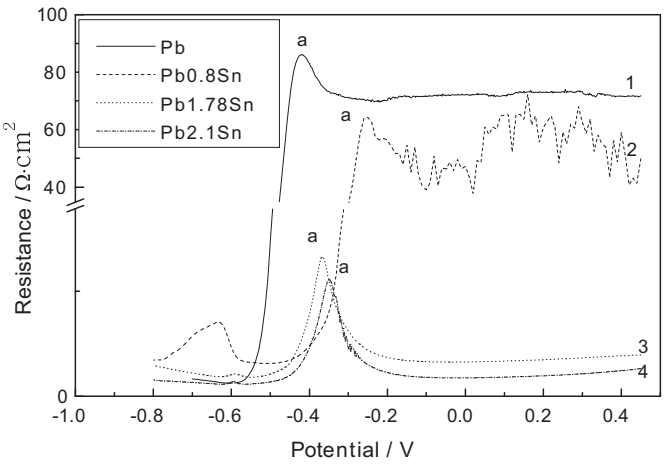


**Fig. 13.** The linear sweeping voltage of anodic films on Pb, Pb0.8Sn, Pb1.78Sn and Pb2.1Sn electrodes at 1.28 V for 2 h in 4.5 M $H_2SO_4$ solution.

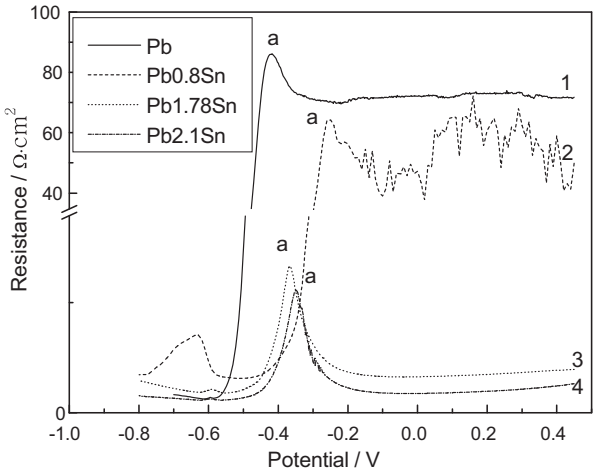


**Fig. 14.** The a.c. voltammetries of the anodic films on Pb0.8Sn alloy at 1.28 V for 2 h in 4.5 M $H_2SO_4$ solution at different temperatures.

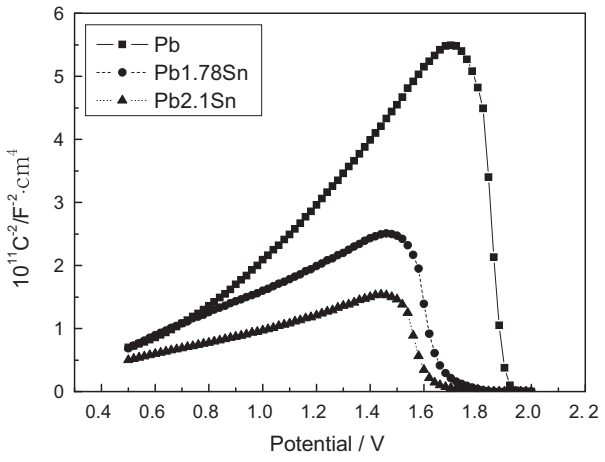


**Fig. 16.** Mott–Schottky plots of anodic films formed on Pb, Pb1.78Sn and Pb2.1Sn electrodes at 1.28 V for 2 h in 4.5 M $H_2SO_4$ solution.

**Table 2**
The fitted results of the impedance spectra.

| Elements | Pb | Pb0.8Sn | Pb1.78Sn | Pb2.1Sn |
|---|---|---|---|---|
| $R_s$ ($\Omega$ cm$^2$) | 0.1528 | 0.4256 | 1.164 | 1.112 |
| $Y_{cdl}$ ($\Omega^{-1}$ $S^n$) | 8.972E−6 | 1.958E−5 | 2.031E−3 | 1.683E−3 |
| $n_{cdl}$ | 1 | 1 | 0.9523 | 0.8826 |
| $R_{ct}$ ($\Omega$ cm$^2$) | 2572 | 1627.2 | 591.6 | 104.3 |
| $Y_{PbSO_4}$ ($\Omega^{-1}$ $S^n$) | 4.194E−6 | 8.476E−5 | 8.476E−5 | 2.344E−4 |
| $n_{PbSO_4}$ | 0.8237 | 0.7986 | 0.8491 | 0.8691 |
| $R_{PbSO_4}$ ($\Omega$ cm$^2$) | 4.525E4 | 2.548E4 | 7249 | 8079 |
| $Y_{PbO}$ ($\Omega^{-1}$ $S^n$) | 6.861E−6 | 1.411E−4 | 2.814E−4 | 5.607E−4 |
| $n_{PbO}$ | 0.947 | 0.938 | 0.9446 | 0.957 |
| $R_{PbO}$ ($\Omega$ cm$^2$) | 3.87E4 | 2.064E4 | 8390 | 6649 |

### 3.2.5. Electrochemical impedance spectroscopy (EIS)

The Nyquist plots of anodic films formed on four electrodes at 1.28 V for 2 h in 4.5 M $H_2SO_4$ solution are illustrated in Fig. 15, it can been observed that the semicircle decreased with the increment of Sn content, it was an indication of the enhanced protection. Similarly, the equivalent electron circuit shown in Fig. 7 was employed to fit the impedance spectra, the results are shown in Table 2, it can be noticed that the resistances of $PbSO_4$ film, PbO film and the transfer resistance decreased, the capacitances of double layer, $PbSO_4$ film and PbO film increased with the increment of Sn content, the increment of capacitance and decrement of resistance implying the decreased film protection. The decrement resistance of PbO film indicated Sn can enhance the conductivity of the anodic film on lead alloy. According to Pavlov et al. [5], the addition of Sn into lead alloys decreased the starting potential of the PbO to $PbO_n$ ($1 < n < 2$) oxidation reaction by approximately 0.2 V, and the decreased potential was due to the action of Sn incorporated in the lead oxide layer. Since tet-PbO and SnO were isomorphous, Sn were readily incorporated in the sublattice of lead oxide and will create the same type of conductivity, then Sn ions exchanged valencies between themselves and probably with $Pb^{3+}$ ions, therefore, the conductivity of the anodic film on lead alloy improved by increasing Sn content, it was in agreement with the potentiodynamic curve and ACV.

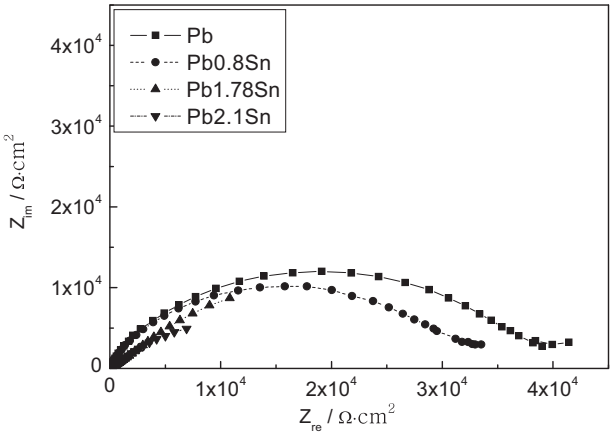


**Fig. 15.** The Nyquist plots of anodic films on Pb, Pb0.8Sn, Pb1.78Sn and Pb2.1Sn electrodes at 1.28 V for 2 h in 4.5 M $H_2SO_4$ solution.

### 3.2.6. Mott–Schottky plot

The capacitance of the anodic films on four electrodes at 1.28 V for 2 h in 4.5 M $H_2O_4$ solution dependence on potential is depicted in Fig. 16, it revealed the slopes of the straight lines in MS plots appeared positive, indicating an n-type semiconductive property of the anodic film. The slope significantly decreased with ascending Sn content. Based on Eq. (4), it can be concluded that the donor density within the anodic film increased with ascending Sn content. According to Pavlov et al. [16], the anodic film formed on lead alloy at 1.28 V was mainly composed of tet-PbO, PbO·$PbSO_4$ and $PbSO_4$, in which tet-PbO had p-type semiconductive character. However, the positive slopes of MS plots meaning the n-type semiconductive performance of the anodic film, therefore, there must existing the oxides with n-type semi-conductive within the anodic film, comparing with ACV and EIS results, the appearance of $PbO_2$ within the anodic film can explain the positive slope in MS plots. Then, it can be obtained that the anodic film on PbSn alloy may be composed of a mixture of PbO and $PbO_2$, the $PbO_2$ content in the anodic film increased with the increment of Sn content.

### 3.2.7. Microstructures of corrosion films after CV

The micro-structure of corrosion films on four PbSn electrodes after CV for 100 cycles in 4.5 M $H_2SO_4$ solution is illustrated in Fig. 17, it was apparent that the corrosion film displayed tetragonal structure, the porosity of the corrosion film increased with ascending Sn content, the porosity can act as the micro-channels of ions diffusion, larger porosity of the corrosion film lower diffusion resistance of ions within the corrosion film was, therefore, the conductivity of the corrosion film on PbSn alloy in 4.5 M $H_2SO_4$ solution was improved by increasing Sn content, this was in agreement with the electrochemical experiments.

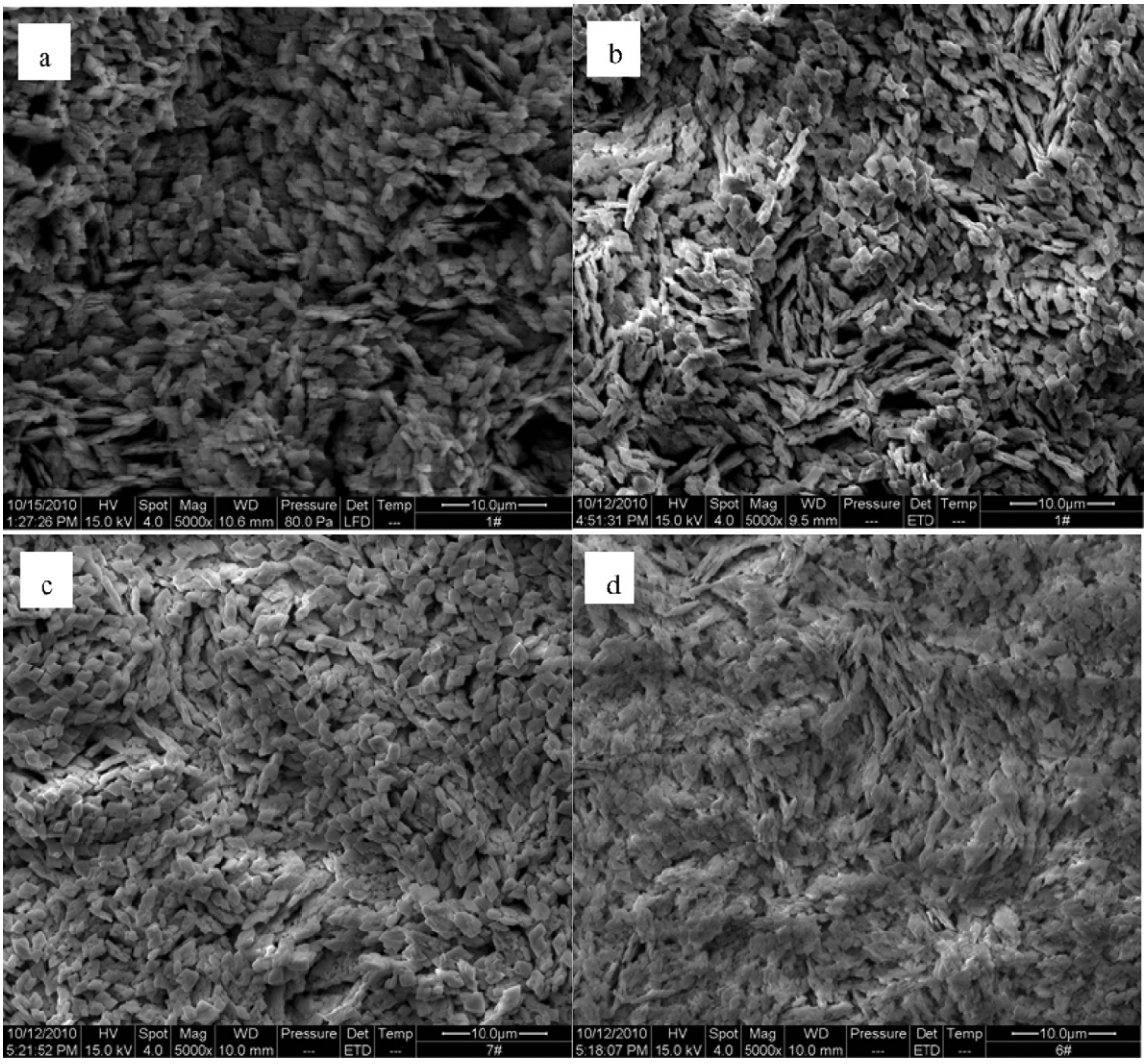


**Fig. 17.** Micro-structure of corrosion films on four PbSn electrodes after CV for 100 cycles in 4.5 M $H_2SO_4$ solution, (a) Pb electrode; (b) Pb0.8Sn electrode; (c) Pb1.78Sn electrode; (d) Pb2.1Sn electrode.

### *3.3. Influence of pH value on corrosion behaviors of Pb0.8Sn alloy in sulfuric acid solution*

#### *3.3.1. Cyclic voltammetry (CV)*

Fig. 18a–d shows the cyclic voltammetries of Pb0.8Sn electrode in 1.5 M, 2.5 M, 3.5 M and 4.5 M $H_2SO_4$ solutions, respectively. On the whole, the cyclic voltammetries measured at different $H_2SO_4$ solutions appeared similar feature, three anodic peaks donated as o, p and q can be observed in the positive scanning process, an apparent reduction peak noted as m arose in the cathodic scanning process, the detailed corresponding reactions of peaks o, p q and m were illustrated in above sections. For the solution with the fixed pH value, three peaks (o, p and m) currents increased with cycle numbers, the reason can be related to the increased corrosion of the electrode and the increasing specific surface area of the corrosion film with cycles. While at one fixed cycle number, all peaks currents decreased with ascending $H_2SO_4$ concentration, it indicating the decreased corrosion.

Likewise, Fig. 19 shows the variation of anodic oxidation charge ($Q_{ox}$), cathodic reduction charge ($Q_{red}$) and the difference between them ($Q_{ox} - Q_{red}$) with cyclic numbers, we can assume the difference between $Q_{ox}$ and $Q_{red}$ may be due to the oxygen evolution, it was observed from Fig. 19 that there were good linear relationships between $Q_{red}/Q_{ox} - Q_{red}$ and the cyclic numbers ($N$). Obviously, the increase rate of reduction and oxygen evolution decreased with the increment of $H_2SO_4$ concentration, implying the declined corrosion and decreased oxygen evolution on Pb0.8Sn alloy in $H_2SO_4$ solution with low pH value.

#### *3.3.2. Potentiodynamic curve*

The influence of $H_2SO_4$ concentration on potentiodynamic curves of Pb0.8Sn alloy in $H_2SO_4$ solution is illustrated in Fig. 20, it revealed that Pb0.8Sn electrode was in the passive state in all kinds of solutions with a passive potential region from about 0.094 V to 1.7 V, the passive potential regions slightly enlarged with increasing $H_2SO_4$ concentration. While for the steady passive currents of Pb0.8Sn electrode in 0.5 M, 1.5 M, 2.5 M, 3.5 M and 4.5 M $H_2SO_4$ solutions, they decreased from 4.75E−4 A $cm^{-2}$, 3.6E−4 A $cm^{-2}$, 3.08E−4 A $cm^{-2}$, 2.42E−4 A $cm^{-2}$ and 1.77E−4 A $cm^{-2}$, respectively. Apparently, the ascending of passive potential region and descending of passive currents demonstrated that the improving of $H_2SO_4$ concentration can enhance the passive performance of Pb0.8Sn in $H_2SO_4$ solution, and then the protection of the passive film on Pb0.8Sn alloy can be increased with $H_2SO_4$ concentration.

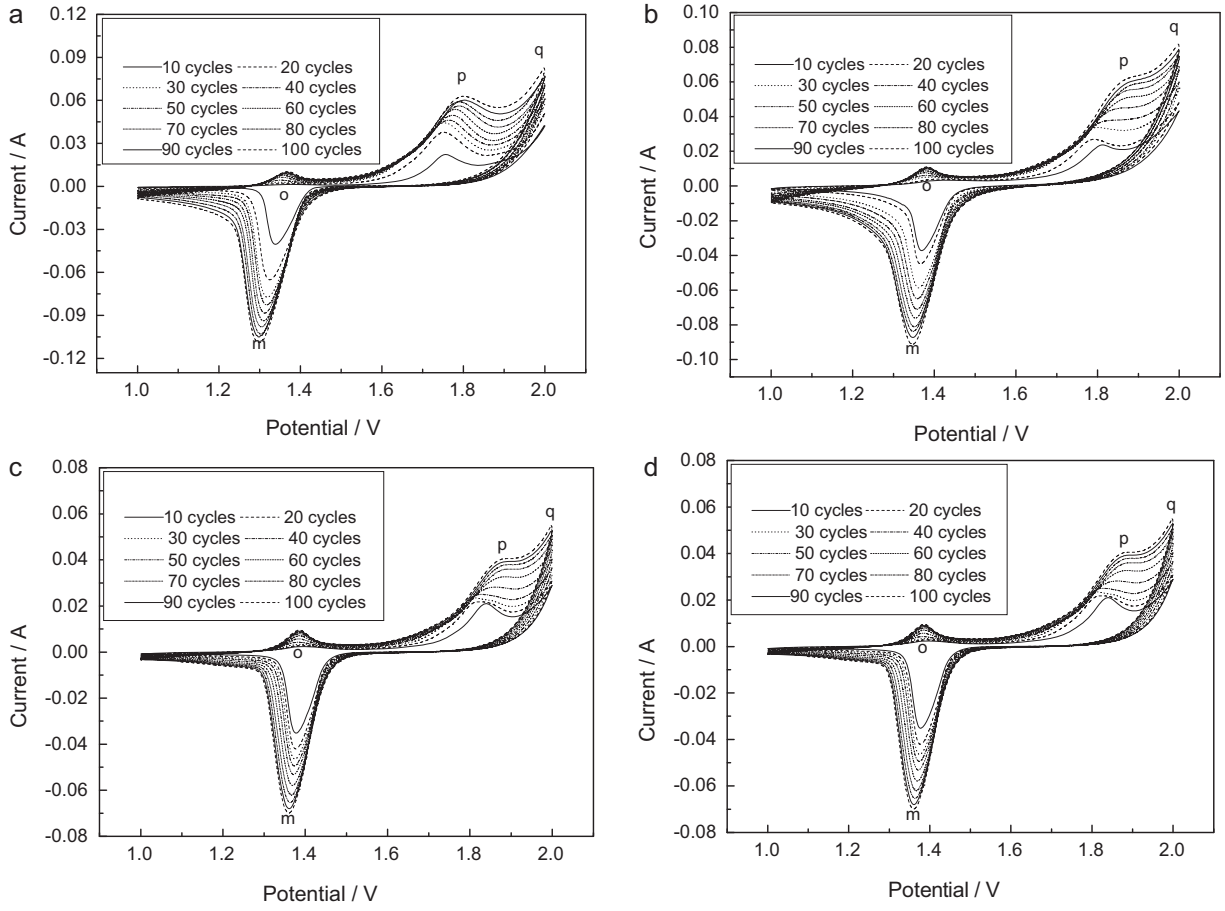


**Fig. 18.** Cyclic voltammetries of Pb0.8Sn electrode in $H_2SO_4$ solution with different pH values, (a) 1.5 M, (b) 2.5 M, (c) 3.5 M and (d) 4.5 M.

*3.3.3. Linear sweeping voltage (LSV)*

The linear sweeping voltammetries of anodic films on Pb0.8Sn electrode at 1.28 V for 2 h in $H_2SO_4$ solutions with different pH values are illustrated in Fig. 21, it was clear that two reduction peaks a and b appeared in LSV, the corresponding currents of peaks a and b increased with increasing $H_2SO_4$ concentration. Considering peaks a and b corresponding to the reduction of Pb(II) (like PbO, $PbO{\cdot}PbSO_4$, $3PbO{\cdot}PbSO_4$, etc.) and $PbSO_4$ to Pb, then, it can be concluded that the growth of Pb(II) in the anodic film was improved by decreasing pH value, as high resistance of PbO, the resistance of the anodic film would be enhanced, and then the film protection increased, this was in agreement with the potentiodynamic curve.

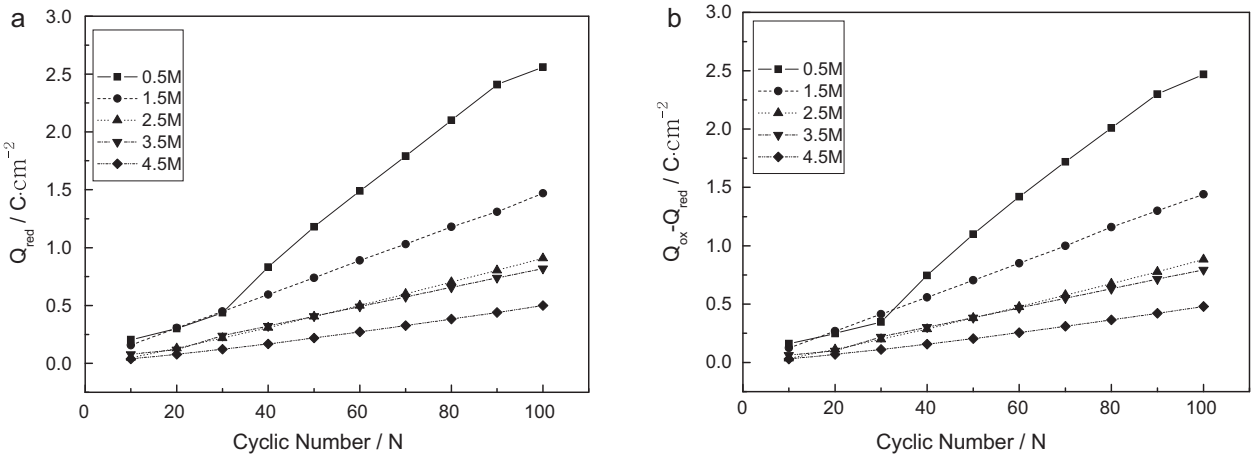


**Fig. 19.** $Q_{red}$ and $Q_{ox} - Q_{red}$ verse cyclic numbers for corrosion films formed on Pb0.8Sn alloys in $H_2SO_4$ solution with different pH values, (a) $Q_{red}$ verse cyclic number plot, (b) $Q_{ox} - Q_{red}$ verse cyclic number plot.

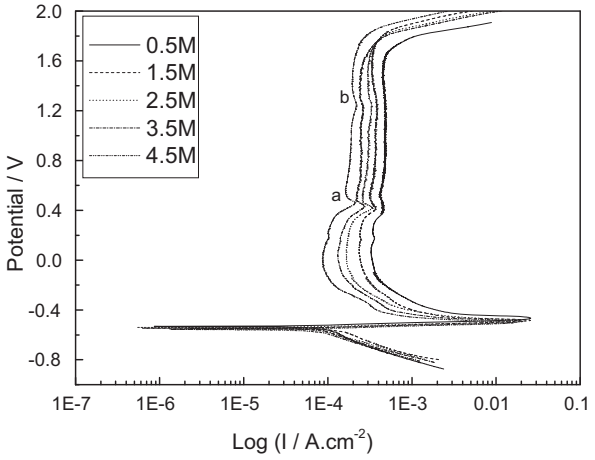


**Fig. 20.** The potentiodynamic curves of Pb0.8Sn electrode in $H_2SO_4$ solutions with different pH values.

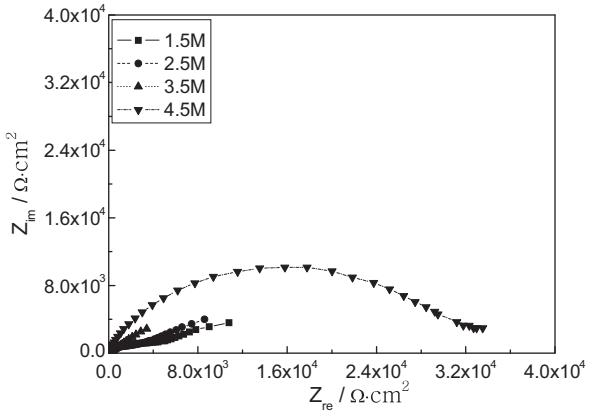


**Fig. 22.** The Nyquist plots of anodic films on Pb0.8Sn electrode at 1.28 V for 2 h in $H_2SO_4$ solutions with different pH values.

### 3.3.4. Electrochemical impedance spectroscopy (EIS)

The Nyquist plots of anodic films formed on Pb0.8Sn electrode at 1.28 V for 2 h in $H_2SO_4$ solutions with different pH values are depicted in Fig. 22, it clearly showed that the semicircle increased with the decreased pH value, it implying the increased film protection. Similarly, the equivalent electron circuit shown in Fig. 7 was used to fit the impedance spectra, the results are shown in Table 3, it can be noticed that the resistances of $PbSO_4$ film, PbO film and the transfer resistance increased, while the capacitances of double layer, $PbSO_4$ film and PbO film decreased with the increment of $H_2SO_4$ concentration, the decrement of capacitance and increment of resistance indicating the increased film protection. The increment resistance of PbO film revealed the decrement of pH value can enhance the protective effect of the anodic film, the reason may be related to the composition changing of the anodic film.

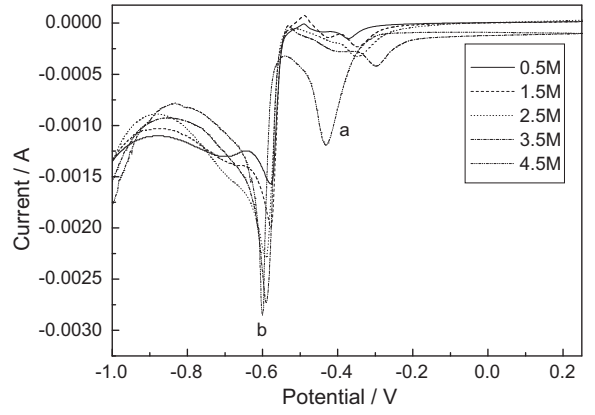


**Fig. 21.** The linear sweeping voltammetries of Pb0.8Sn electrode in $H_2SO_4$ solutions with different pH values.

**Table 3**
The fitted results of the impedance spectra.

| Elements | 1.5 M | 2.5 M | 3.5 M | 4.5 M |
|---|---|---|---|---|
| $R_s$ ($\Omega$ cm$^2$) | 1.062 | 0.9976 | 0.7315 | 0.4256 |
| $Y_{cdl}$ ($\Omega^{-1}$ S$^n$) | 6.249E−4 | 6.567E−4 | 2.197E−4 | 1.958E−5 |
| $n_{cdl}$ | 0.768 | 0.8615 | 0.8547 | 1 |
| $R_{ct}$ ($\Omega$ cm$^2$) | 16.91 | 177.2 | 199.4 | 1627.2 |
| $Y_{PbSO_4}$ ($\Omega^{-1}$ S$^n$) | 4.52E−4 | 2.398E−4 | 2.413E−4 | 8.476E−5 |
| $n_{PbSO_4}$ | 1 | 0.8238 | 0.8063 | 0.7986 |
| $R_{PbSO_4}$ ($\Omega$ cm$^2$) | 1.084E4 | 1.106E4 | 1.517E4 | 2.548E4 |
| $Y_{PbO}$ ($\Omega^{-1}$ S$^n$) | 4.899E−4 | 4.065E−4 | 3.277E−4 | 1.411E−4 |
| $n_{PbO}$ | 0.7355 | 0.8651 | 0.8493 | 0.938 |
| $R_{PbO}$ ($\Omega$ cm$^2$) | 1.109E4 | 1.736E4 | 1.938E4 | 2.064E4 |

Takehara and Kanumura [30,31] studied the $H_2SO_4$ concentration effect on the processes of $PbSO_4$ oxidation to $PbO_2$, they found that the oxidation rate of $PbSO_4$ increased with ascending $H_2SO_4$ concentration. The fitted results revealed that the Pb(II) resistance increases with increasing $H_2SO_4$ concentration, that was the growth of high resistance PbO film was encouraged with descending pH value, according to Takehara and Kanumura [31], the oxidation of $PbSO_4$ was written by the following equation:

$$PbSO_4 \rightarrow Pb^{2+} + SO_4^{2-} \quad (5)$$

$$Pb^{2+} + 2H_2O \rightarrow PbO_2 + 4H^+ + 2e \quad (6)$$

Based on chemical equilibrium, decreasing pH value can be beneficial to the growth of $PbO_2$, therefore, the $PbO_2$ content in the anodic film on lead alloy will increase, and then the film conductivity enhanced with decreasing $H_2SO_4$ concentration, this reflected in the Nyquist plot by a shrinked semicircle with decreasing $H_2SO_4$ concentration.

### 3.3.5. Microstructures of corrosion films after CV

The micro-structure of corrosion films on Pb0.8Sn electrode after CV for 100 cycles in $H_2SO_4$ solutions with different pH values is illustrated in Fig. 23, apparently, the corrosion film displayed tetragonal structure, the porosity of the corrosion film decreased with ascending $H_2SO_4$ concentration, the porosity can act as the micro-channels of ions diffusion, larger porosity of the corrosion film lower diffusion resistance of ions within the corrosion film was, therefore, the film protection improved with increasing $H_2SO_4$ concentration, this was in agreement with the electrochemical experiments.

## 4. Conclusions

Temperature, Sn content and $H_2SO_4$ concentration played an important role in determining the corrosion behaviors of PbSn alloy and the conductivity of the anodic film on PbSn alloy at 1.28 V in sulfuric acid solution. The corrosion resistance of PbSn alloy in sulfuric acid solution was improved by decreasing temperature, increasing Sn content and $H_2SO_4$ concentration; the conductivity of anodic

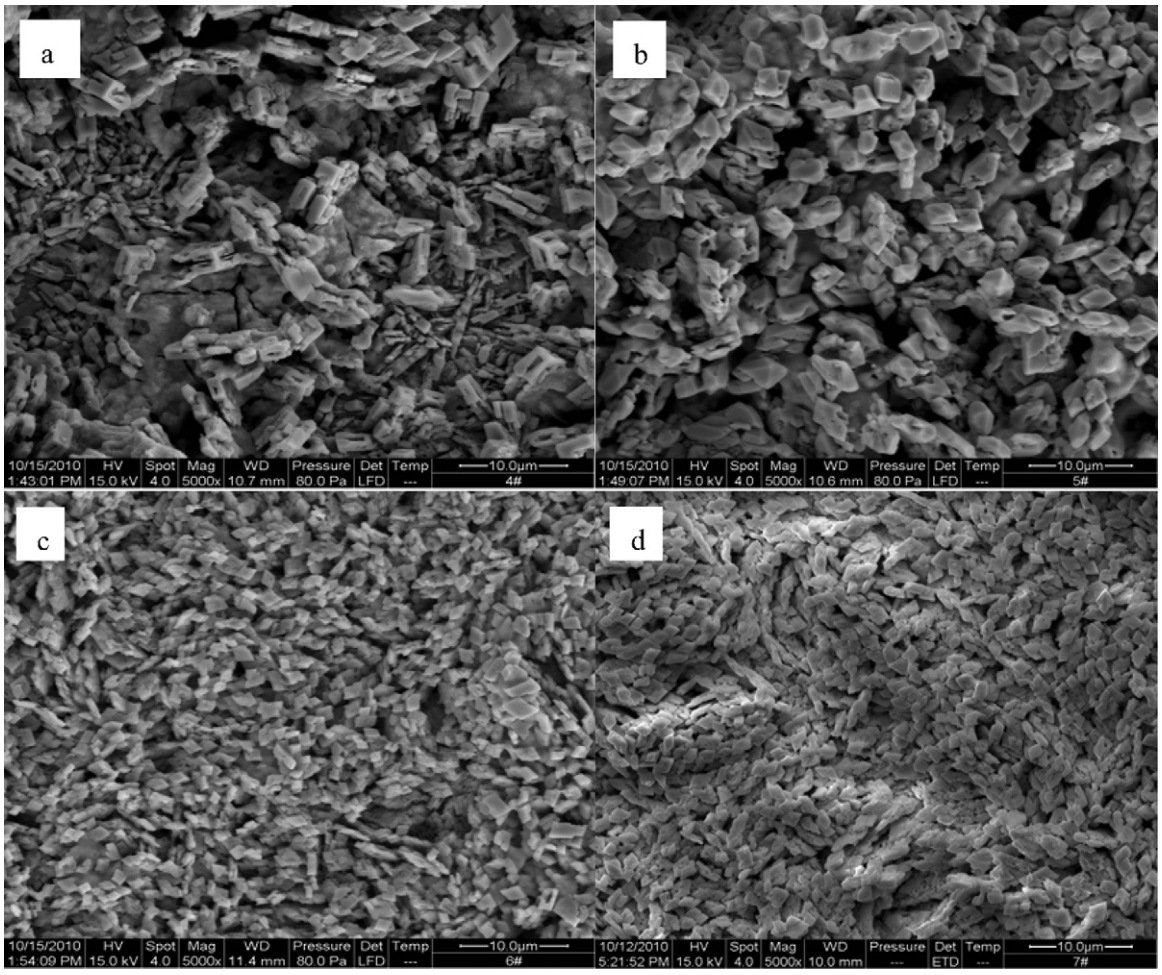


**Fig. 23.** Micro-structure of corrosion films on four PbSn electrodes after CV for 100 cycles in different $H_2SO_4$ solutions, (a) 1.5 M; (b) 2.5 M; (c) 3.5 M; (d) 4.5 M.

films on PbSn alloys was enhanced with increasing temperature, ascending Sn content and descending $H_2SO_4$ concentration.

## References

[1] D. Pavlov, in: B.D. McNicol, D.A.J. Rand (Eds.), Power Sources for Electrical Vehicles, Elsevier, Amsterdam, 1984.
[2] R.D. Prengaman, J. Power Sources 95 (2001) 224.
[3] R.D. Prengaman, J. Power Sources 53 (1995) 207.
[4] L.C. Peixoto, W.R. Osório, A. Garcia, J. Power Sources 192 (2009) 724.
[5] D. Pavlov, B. Monakhov, M. Maja, N. Penazzi, J. Electrochem. Soc. 136 (1989) 27.
[6] M. Bojinov, B. Monahov, J. Power Sources 39 (1990) 287.
[7] W.R. Osório, L.C. Peixoto, A. Garcia, J. Power Sources 195 (2010) 1726.
[8] D.G. Li, G.S. Zhou, J. Zhang, M.S. Zheng, Electrochim. Acta 52 (2007) 2146.
[9] R.K. Shervedani, A.Z. Isfahani, R. Khodavisy, A.H. Mehrjardi, J. Power Sources 164 (2007) 890.
[10] J.L. Caillerie, L. Albert, J. Power Sources 67 (1997) 279.
[11] D. Pavlov, J. Power Sources 42 (1993) 345.
[12] A.F. Hollenkamp, J. Power Sources 36 (1991) 567.
[13] E. Meissner, J. Power Sources 46 (1993) 231.
[14] D. Pavlov, J. Power Sources 48 (1994) 179.
[15] A.F. Hollenkamp, J. Power Sources 59 (1996) 87.
[16] D. Pavlov, C.N. Poulieff, E. Klaja, N. Jordanov, J. Electrochem. Soc. 116 (1969) 316.
[17] K. Takahashi, N. Hoshihara, H. Yasuda, T. Ishii, H. Jinbo, J. Power Sources 30 (1990) 23.
[18] B.J. Carter, S.D. Stefano, L. Whitcanack, Ext. Abstr. No. 94, vol. 86–2, The Electrochemical Society, Pennington, NJ, USA, 1986, p. 133.
[19] R.F. Nelson, D.M. Wisdom, J. Power Sources 33 (1991) 165.
[20] A.J. Debethune, T.S. Licht, Wsendeman, J. Electrochem. Soc. 106 (1959) 616.
[21] H.T. Liu, J. Yang, H.H. Liang, J.H. Zhuang, W.F. Zhou, J. Power Sources 93 (2001) 230–233.
[22] J. Han, C. Pu, W.F. Zhou, J. Electroanal. Chem. 368 (1994) 43.
[23] J. Hubrecht, M. Embrechts, W. Bogaerts, Electrochim. Acta 38 (1993) 1867.
[24] M. Cai, S.M. Park, J. Electrochem. Soc. 143 (1996) 3895.
[25] L. Hamadou, A. Kadri, N. Benbrahim, Appl. Surf. Sci. 252 (2005) 1510–1519.
[26] H.W. Wilson, J. Appl. Phys. 48 (1977) 4292.
[27] J.F. Dewald, J. Phys. Chem. Solids 14 (1960) 155.
[28] M. Bojinov, K. Solmi, G. Sundholm, Electrochim. Acta 39 (1994) 719.
[29] K. Wiesener, J. Garche, N. Anastasijevic, J. Power Sources 9 (1983) 17.
[30] Z. Takehara, K. Kanumura, J. Electrochem. Soc. 134 (1987) 1604.
[31] Z. Takehara, K. Kanumura, J. Electrochem. Soc. 134 (1987) 13.